ORIGIN OF JUPITER'S DECAMETRIC MODULATION LANES

K. Imai*, L. Wang†, and T. D. Carr†

Abstract

Although it has been more than two decades since the discovery of the modulation lanes in the dynamic spectra of Jupiter's decametric radiation by Riihimaa, a realistic model accounting for them has not yet been published. We present such a model for modulation lanes observed during Io–A and Io–B storms. A grid–like interference screen composed of field–aligned columns of enhanced plasma density downstream from Io is assumed. The screen is located at the inner edge of the Io plasma torus, the columns crossing Io's orbit. The column spacing is on the order of 100 km. Radiation from the source near the northern foot of the Io–activated flux tube passes through the screen on its way to Earth. Interference between rays that are scattered on passing through the columns with the relatively unscattered rays passing between columns produces a multilobed radiation intensity pattern that rotates with slightly less than Jupiter's angular velocity. Emission at different frequencies is produced at different altitudes above the foot of the activated flux tube, and because of its slope, at slightly different longitudes. Within a received bandwidth at Earth, some frequency components will have arrived from intensity lobe maxima and others from lobe minima. The frequency–time plot is thus in the form of characteristically sloping modulation lanes. Our model provides remarkably close fits to the best available modulation lane observations, and also yields values of both the lead angle of the radio–emitting flux tube ahead of Io and the cone half–angle of the assumed hollow–cone emission beam.

1 Introduction

Jupiter's decametric radiation has been extensively observed both from the ground and from spacecraft since its discovery in 1955 (see, for example, Carr and Desch [1976], Carr et al. [1983], and references therein). This radiation is by far the most powerful of the radio emissions from solar system planets. The emission is generally believed to be produced by a mechanism related to the cyclotron maser plasma instability [Wu and

*On leave from Department of Electrical Engineering, Kochi National College of Technology, Nankoku, Kochi 783, Japan.

†Department of Astronomy, University of Florida, Gainesville, Florida 32611, USA

Lee, 1979] that is apparently responsible for the terrestrial kilometric radiation. There is considerable evidence indicating that the Jovian radiation originates in the northern auroral zone (and perhaps to a much lesser extent in the southern zone) at altitudes above the cloud tops at which the electron cyclotron frequencies are only slightly less than the frequencies being emitted.

Frequency–time dynamic spectra of Jupiter's emissions display a high degree of complexity, exhibiting intricate structure on several widely different time scales. The L–bursts, with durations usually between 1 and 10 sec are the most common type observable from Earth. It has long been known that the modulation envelope characterizing individual L bursts has been impressed upon Jovian bursts of much longer intrinsic durations by scintillation due to the rapidly drifting inhomogeneities in the interplanetary plasma along the ray path [Douglas and Smith, 1961; 1967]. This modulation pattern is disordered, and its frequency dependence is hardly apparent in relatively narrow band dynamic spectra [Genova et al., 1981].

There is an additional modulation component known as the modulation lanes, which were discovered by Riihimaa [1968; 1970]. The characteristic spectral pattern of this modulation, in contrast to those of L–bursts, is relatively well ordered and is strongly frequency dependent, even when relatively narrow bandwidths are observed. In this paper we show that the major component of the Jovian modulation lane structure is probably impressed upon escaping Jovian radiation by constructive and destructive interference due to some type of regular striated structure in the part of the Io plasma torus through which the radiation passes, and that the frequency drifts of the modulation lanes are due to the relative inclination and motion of this interfering structure with respect to the radio–emitting part of the active flux tube. We present a model for such a structure consisting of an interference screen composed of parallel columns of increased plasma density that are aligned with the Jovian magnetic field; the model has been adjusted to provide a close fit to observed data.

It is customary to display Jovian dynamic spectra as gray–scale brightness plots in which the time axis is horizontal and the frequency axis is vertical. Modulation lanes appear on such dynamic spectra as parallel sloping narrow bands that are alternately bright and dark. The lane slopes can be either positive or negative. The sloping lanes pass undeviated from one L burst to another. Although adjacent L burst regions are also separated by dark lanes, these lanes are vertical; L–burst structure is relatively independent of frequency. After his discovery of modulation lanes, Riihimaa [1970; 1974] showed that their slopes are strongly correlated with Jupiter's central meridian longitude (CML, *System III*), indicating that this modulation component originates in the Jovian magnetosphere rather than in the interplanetary medium or in the terrestrial ionosphere. (There is, in fact, an additional modulation lane component due to the effect of Earth's ionosphere, but it is easily recognizable [Genova et al., 1981] and has not led to erroneous conclusions regarding the intrinsic Jovian modulation lanes.)

Riihimaa [1976] also demonstrated, and Genova et al. [1981] verified, that there is no marked difference between the Jovian modulation lane dynamic spectra obtained using right hand and left hand circularly polarized antennas, respectively. In their investigation of the modulation lane phenomena, Genova et al. [1981] employed a spectrograph

having much wider bandwidth and higher sensitivity than Riihimaa's spectrograph, revealing modulation lane phenomena in broader scope and greater detail. However, these observations cover a much smaller time span than do those of Riihimaa [1978]. The plot of modulation lane frequency drift rate vs CML by Riihimaa [1978], based on 10 years of observations between 21 and 23 MHz, provides the best available statistical results of this type for the modulation lanes occurring during Io–related storms, and is the principal basis for the development of the model presented in this paper.

Riihimaa [1974] suggested that the modulation lanes are impressed upon the escaping Jovian radiation as it passes through parallel slots in an otherwise opaque screen located in the boundary region between the magnetosphere of the planet and the interplanetary medium (the Io plasma torus had not been discovered at this time). In Riihimaa's model, the geometrical relationship between the radio–emitting flux tube and the slots in the screen resulted in the opposite frequency–time drifts of Io–B and Io–A radio sources that are actually observed. Zheleznyakov and Shaposhnikov [1979] proposed a modulation lane model based on the Faraday effect for propagation in a plasma in a direction transverse to the magnetic field. This model predicted a difference in the modulation lanes as observed with left– and right–hand polarized antennas. The above–mentioned finding that there is no such polarization effect led to the rejection of this model. Meyer–Vernet et al. [1981] and Genova et al. [1981] considered diffraction of the radiation as it passes through the Io plasma torus in connection with the production of modulation lanes, but proposed no detailed model that could be tested against observed data. The only similarity of the model we present in this paper to that of Riihimaa is in regard to his geometrical explanation of the opposite frequency–time drifts of the Io–B and Io–A sources (although instead of Riihimaa's idea of transmission through a slotted screen located near the magnetopause we assume ray interference from field–aligned plasma striations in the Io torus). Also, our model bears little similarity to the mechanism suggested by Meyer–Vernet et al. other than that it is due to a multipath interference effect taking place in the Io torus.

2 Phenomenology

Terrestrially observed Jovian decametric emission usually occurs in clearly defined storms which are classified into four principal source regions on the CML–Io phase plane. These are designated Io–B, Io–A, Io–C, and Non–Io–A. Io–B occurs when Io's orbital position is within a range centered near 90° Io–phase (the angle measured eastward from *superior geocentric conjunction*, SGC); the Io phase ranges for Io–A and Io–C are both centered near 240° from SGC. For Non–Io–A storms Io's phase can lie anywhere outside the Io–A range. The most predictable storms are of types Io–B and Io–A. Most of the available modulation lane data are for these two types, although the lanes also occur during Io–C and Non–Io–A storms as well. In this paper we shall be concerned only with modulation lanes that have been observed during Io–B and Io–A storms.

At frequencies in the vicinity of 22 MHz, most modulation lane patterns have frequency drift rates between +100 and +180 kHz/sec for Io–B storms and between −90 and −150 kHz/sec for Io–A storms. The lanes generally display a strong periodicity in time, with

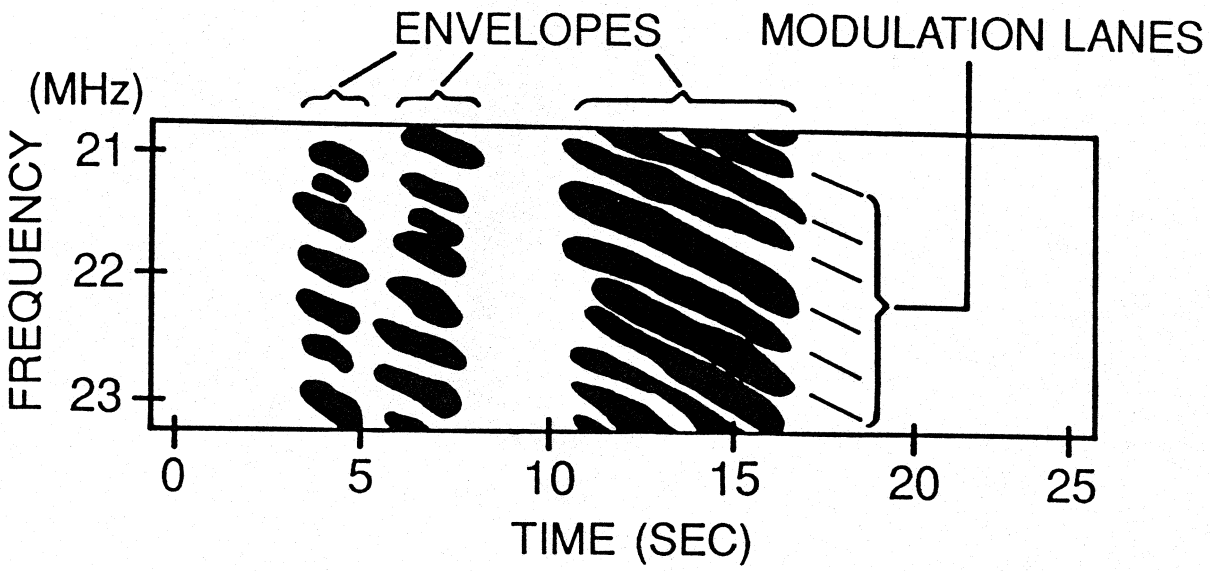

Figure 1: Idealized dynamic spectrum illustrating modulation envelopes and positively drifting modulation lanes (after Riihimaa, [1971]).

Table 1: Characteristics of Modulation Lanes at about 23 MHz

	Component	Drift Sense	Most Probable Drift Rate	Mean Time Spacing
Io–B Source	Major	Positive	$125 \sim 150$ kHz/sec	2 sec
	Minor	Negative	$-25 \sim -50$ kHz/sec	10 sec
Io–A Source	Major	Negative	$-100 \sim -150$ kHz/sec	2 sec
	Minor	Positive	$15 \sim 25$ kHz/sec	10 sec

periods ranging from about 1 to 5 sec and an average of about 2 sec. Figure 1 is a sketch illustrating a typical set of positively drifting modulation lanes in which L–burst structure is also apparent. We shall refer to the modulation lanes possessing drift rates and periodicity within the above ranges as the major component. There is a minor modulation lane component, representing a considerably smaller fraction of the total number observed, for which the drift rates are of opposite sign than for the major component or are of the same sign but of smaller absolute value. For these cases the lanes are usually broader and their separations in time are longer. Table 1 is a summary of characteristics of modulation lanes at frequencies in the vicinity of 23 MHz observed by Genova et al. [1981]. This table shows the significant differences of characteristics between the major and the minor components of modulation lanes. Minor component lanes are apparently of somewhat different origin from major component lanes; our model applies only to the latter.

It is generally agreed that Io–B and Io–A emission originates from the same general region of the northern Jovian auroral zone. The radiation is emitted into a thick curved sheet that is more or less in the form of a hollow cone. It is composed of ray vectors making angles somewhat less than 90° with respect to the magnetic field in the region. Io–B activity is

observed when one limb of the hollow cone intersects the Earth direction, and Io–A when the other limb of the cone is toward Earth. Two conditions for emission to occur are: *a*) The emitting region at a given time, located near the foot of the flux tube passing through it, must be receiving Alfvén wave energy which was introduced into the flux tube as it was carried by magnetospheric corotation past Io somewhat earlier, and *b*) this emitting region must lie within the so–called active longitude zone centered more or less on the Jovian north magnetic pole. As new flux tubes sweep by Io in succession, the resulting Alfvén wave energy introduced into them propagates down to the emission region, so that the emission process continues until the boundary of the active longitude zone has been crossed. Thus as long as the radio emitting region is active, its Jovian longitude leads the sub–Io longitude by a more or less fixed amount. The value of this lead angle has not been directly measured, because of the lack of knowledge of the mean velocity of the Alfvén waves in the Io flux tubes. Hashimoto and Goldstein [1983] estimated the values to be in the vicinity of 20°, on the basis of a model in which the Alfvén wave is first reflected from the ionosphere at the southern foot of the flux tube before exciting radio emission from near the northern foot. We will refer to the flux tube passing through Io at a given time as the *Io flux tube* (IFT), and to the flux tube from the foot of which radiation is being emitted at the same time as the *previously energized flux tube* (PEFT).

3 Model assumptions

We develop a modulation lane model in which the radiation emitted at each frequency is modified by constructive and destructive interference on passing through and between field aligned striations or columns of enhanced plasma density in the Io plasma torus on its way toward Earth. It will be shown that the resulting rotating multilobed pattern of intensity vs magnetic longitude and latitude can account very well for the observed modulation lanes. We feel more certain, however, that modulation lanes result from our derived pattern (or from a very similar one) than we are of the detailed correctness of our proposed model for obtaining this pattern. In other words, we leave open the possibility that a more realistic model for producing the required intensity vs magnetic longitude pattern might be found.

In order to explain the regularity of an observed set of modulation lanes, it is necessary to postulate some degree of regularity in the characteristics and spacing of the scattering field aligned columns. Each scattering column must extend far enough along its flux tube that rays from the sources within the range of altitudes above the magnetic equator that correspond to the frequencies present in the resulting set of modulation lanes can pass through it on their way to Earth. The columns must thus extend to altitudes of about 1 R_J above the magnetic equator in order that observed sets of modulation lanes covering different frequency ranges can be explained. We also assume that the columns are arranged in single file, i.e., in a single layer. We believe that the columns result in some way directly or indirectly from Io's volcanic activity. Perhaps it is a common occurrence for individual gas clouds to be ejected from Io's atmosphere at more or less regular intervals. Each cloud would then be carried downstream by the passing magnetospheric plasma. After becoming ionized the cloud is locked within the magnetic flux tube in which it finds

itself. Free to diffuse along the field lines but not across them, the newly created plasma begins to fill the flux tube, creating a plasma column. Successive ejected clouds would thus produce the row of more or less equally spaced plasma columns. We favor such an explanation at the present time. It is consistent with the observed fact that Io–B source modulation lanes occur more often, are more regular, and are modulated more deeply than those from Io–A source. The elapsed time since Io passed through the part of the torus penetrated by Io–A rays is several hours greater than the elapsed time since Io was in the region penetrated by Io–B rays. The older plasma columns in the path of Io–A radiation may thus have had time to drift outside their original flux tubes and therefore produce less deeply modulated lanes than do the fresher columns through which the Io–B radiation passes.

There are other possible explanations of the field aligned columns in the torus. One that we have considered is some sort of wave propagating approximately perpendicular to the magnetic field and to the line of sight. The total electron content in this case would vary periodically as the wave propagates across the line of sight. If it is assumed that the velocity of this wave is small compared to the magnetospheric corotation velocity at its location, the wave might produce the same effect on the radiation passing through it as would the previously postulated row of field–aligned plasma columns. Magnetosonic waves meet the requirement of propagating nearly normally with respect to the magnetic field, but it appears that their wavelengths would be too small for our model.

Still another possibility we have considered is that the intensity pattern is simply scintillation from a widespread random distribution of field–aligned plasma inhomogeneities in the Io torus (not concentrated within columns). There is no doubt that the scattering centers would be elongated parallel to the field lines, since that is the only direction in which appreciable diffusion can occur. The instantaneous directions of interference maxima and minima would be more widely separated in two–dimensional scintillation patterns within planes parallel to the field lines than within planes perpendicular to the field. Thus the three–dimensional scintillation pattern would consist of elongated (but ever–changing) regions of increased and decreased intensity, with the elongations of the constant–intensity contours being parallel to the magnetic field in the scattering region. As it more or less gradually changes form, the pattern would corotate with the plasma. One would expect the length–to–width ratio of the pattern elongations to be about the same as that of the typical field–elongated scattering center. If a particular scintillation pattern persists on a time scale of tens of seconds, as it does for the terrestrial ionosphere, we believe that rudimentary modulation lanes could be produced over the frequency bandwidth within which the pattern is relatively unchanged. The mechanism of production of these scintillation modulation lanes would be the same as that of the postulated field–aligned plasma columns, to be explained later in this paper. While this model surely could not account for the occasional sets of highly regular modulation lanes covering a frequency band up to 10 MHz, it could perhaps explain the more common occurrences of relatively narrow band and more irregularly spaced sloping lanes.

We now return to the field–aligned plasma column model. Whatever the cause of the columns may be, we assume that when Jovian decametric radio emission happens to pass through a column system in propagating toward Earth, a multilobed interference pattern

may under certain circumstances be produced which leads to observable modulation lanes. We will use the column spacing and density as adjustable parameters in developing our model for the production of modulation lanes. We shall show that there is a particular spacing of the columns that would best produce the required multilobed pattern. The existence of this particular spacing may at first appear to be a highly improbable occurrence. It is less improbable if we assume that while a variety of spacings may occur at different times, it is only those times during which the spacing is within a given range that regular sets of modulation lanes are observed. Extensive sets of well developed lanes after all are rare.

4 Details of the model

We first describe our idealized model for the production of the multilobed intensity pattern at each frequency, after which it will be explained how these lobes give rise to the sloping modulation lanes. We assume that the more closely the actual distribution of plasma columns approaches the idealized model presented here, the more regular becomes the resulting set of lanes. We begin with a brief review of the overall geometry. Figure 2 shows the relationship between Jupiter, Io, and the radio source when Io–B radiation is being emitted toward Earth. The interference screen in the torus consisting of equally spaced plasma columns crossing Io's orbit is also shown. It should be pointed out that the field lines passing through the plasma columns are far removed from the field line

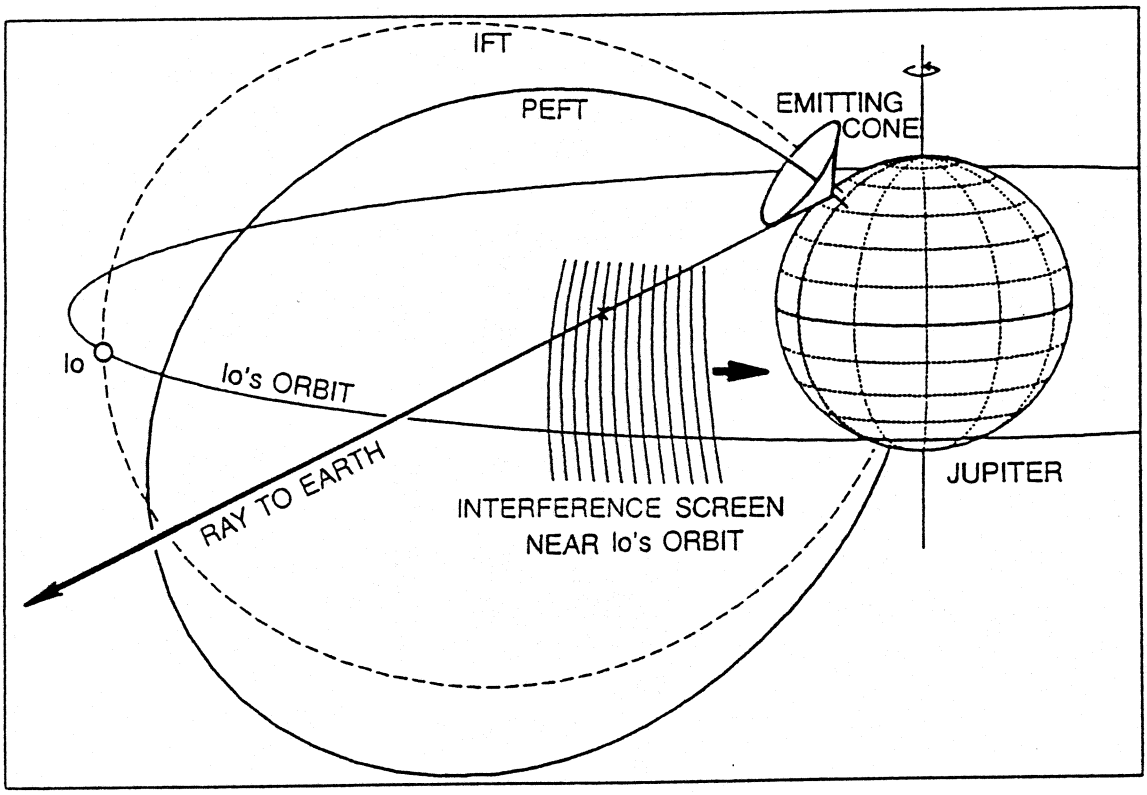

Figure 2: Geometry of our model for the production of modulation lanes. IFT and PEFT are the abbreviations for 'flux tube' and 'previously energized flux tube', respectively.

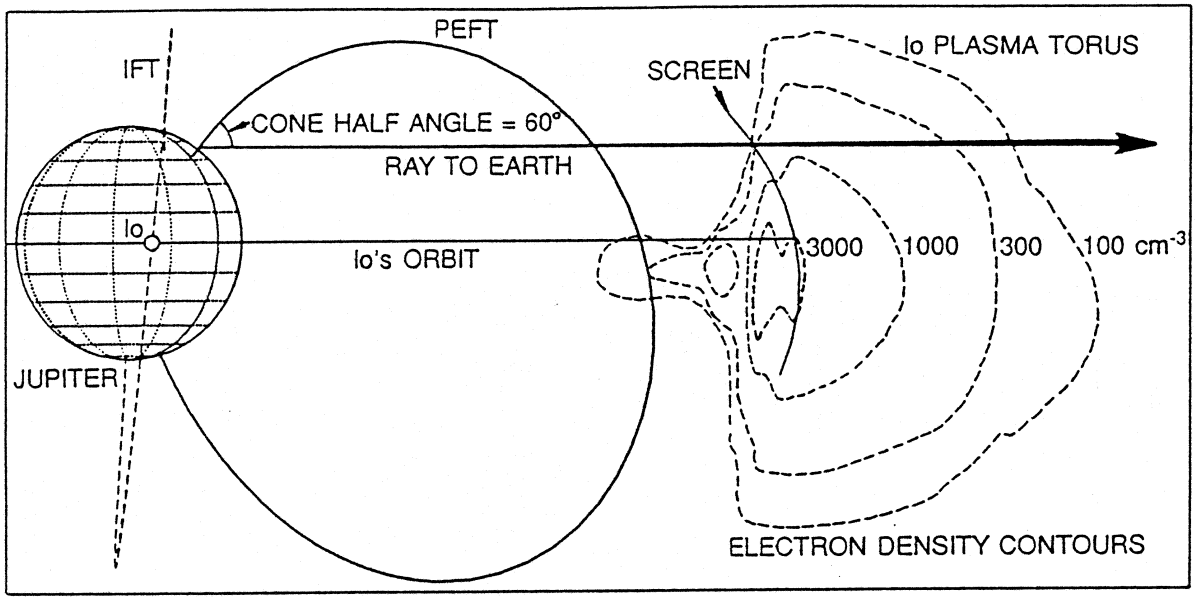

Figure 3: Section through meridian of Io. Electron density contours of the Io plasma torus and the interference screen site are indicated.

passing through the radio source. Figure 3 includes contours of electron number density based on the standard model for the torus, as determined from Voyager measurements . The radio source at a given frequency and time is located at the apex of the thick–walled hollow–cone emission beam, at a given altitude within the previously energized Io flux tube (PEFT). This flux tube is separated from the one currently penetrating Io by a longitude interval of 49°, more or less. Figure 4 is a view from above Jupiter's north pole. The radio source (assumed to be a point) is fixed relative to Io's orbital position, not relative to Jovian longitude. The plasma torus and the flux tubes through it, on the other hand, are fixed in Jovian longitude.

Radiation passing through each plasma column is scattered by the random inhomogeneities present in the electron density distribution. Rays passing between columns are also scattered to a slight degree by the much lower–density background plasma present there, but we assume this intercolumn scattering to be negligible in comparison with that inside each column. The scattering angle, θ radians, is given very approximately by the equation [Kraus, 1986]

$$\theta \approx \left(40.5/f^2\right)\sqrt{w/s}\,\Delta N, \tag{4.1}$$

where f is the frequency, w is the width of a column, s is a typical thickness of the plasma inhomogeneities inside a column, and ΔN is the mean fluctuation of their electron densities; MKS units are used unless otherwise indicated. In this approximate relation, we will interpret θ to be the scattering angle at which the E field is one–half that in the unscattered direction (i.e., the intensity is one–fourth).

Figure 5 is a diagram (not to scale) suggesting the scattering of several rays passing through columns, and others passing unscattered between columns. Some of the rays that have been scattered by three of the columns are indicated by a, b, and c, with subscripts. Rays a_3, b_3, and c_3 have emerged in the unscattered directions. Let us

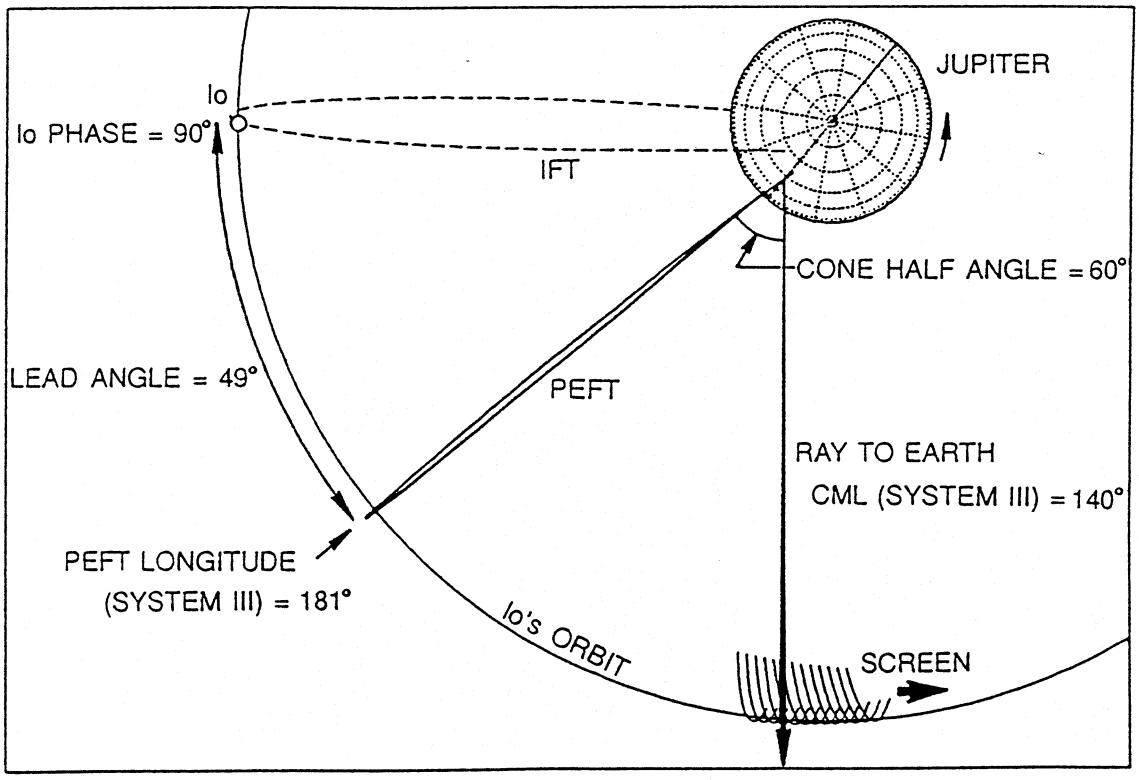

Figure 4: View from above the north pole. A 49° lead angle is illustrated, based on a 60°–half–angle beaming cone.

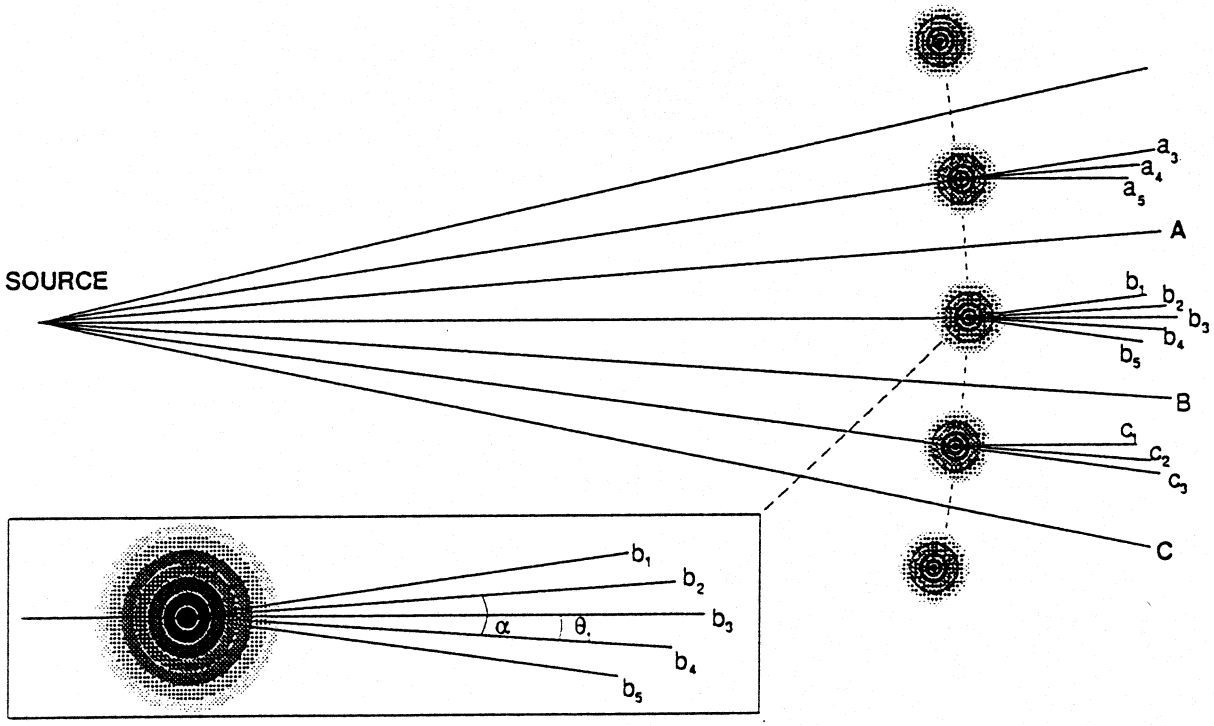

Figure 5: A diagram (not to scale) suggesting the scattering of several rays passing through columns, and others passing unscattered between columns.

assume that scattered rays with subscripts 2 or 4 are at the angle $\theta = \theta_1$ with respect to the corresponding unscattered directions (for the given values $\Delta N = \Delta N_1$ and $f = f_1$), and that those with subscripts 1 or 5 are at the angle $2\theta_1$. Rays A, B, and C pass unscattered between columns.

The members of a group of rays that reach a point on Earth are essentially parallel because the distance to Earth is so much greater than the intercolumn distance; they therefore have plane constant–phase wavefronts. Since we have assumed a point source for the radiation, the phase relationships between the members of such a group reaching Earth have been established largely by the differences in their path lengths between the source and the row of scattering columns. (We neglect another relatively small contribution to their phase differences that is introduced during the scattering process within a column; this is due to differences in the quantity *path phase change minus that over the same path length in free space.*) In Figure 5, those groups of the labeled rays that are parallel are:

__, a_3, and b_1; a_4, A, and b_2; a_5, b_3, and c_1; b_4, B, and c_2; b_5, c_3, and __.

Now let us assume that for a particular frequency $f = f_1$ and a particular column spacing:

1. Rays a_4 and b_2 are in phase with each other, but are 180° out of phase with A.
2. Rays a_5, b_3, and c_1 are all in phase, since a_5 and c_1 have each traveled one wavelength farther than b_3.
3. Rays b_4 and c_2 are in phase, but are 180° out of phase with B.
4. Rays b_1, b_2, b_3, b_4, and b_5 are all separated by the angle θ_1, and their E fields are approximately in proportion to the numbers 0.3, 0.5, 1.0, 0.5, and 0.3, respectively.

It follows that:

1. Rays a_4 and b_2 together nearly cancel A, giving a deep minimum in the intensity pattern at the angle θ_1 from a_3, i.e., midway between a_3 and b_3.
2. Rays a_5 and c_1 reinforce b_3, augmenting the maximum in the intensity pattern in the direction of b_3.
3. Similar relationships exist elsewhere for corresponding rays.

For other frequencies near f_1, the directions of the maxima and minima will be unchanged but the degree of ray reinforcement and cancellation will be reduced. The amount of this reduction will be greater the farther the frequency is from f_1. We will refer to f_1 as the optimum frequency for a given column spacing.

In summary, at all frequencies the intensity maxima are centered on the directions of the column centers and the minima are centered midway between columns. The modulation depth is greatest at the optimum frequency f_1 for a given column spacing. The column

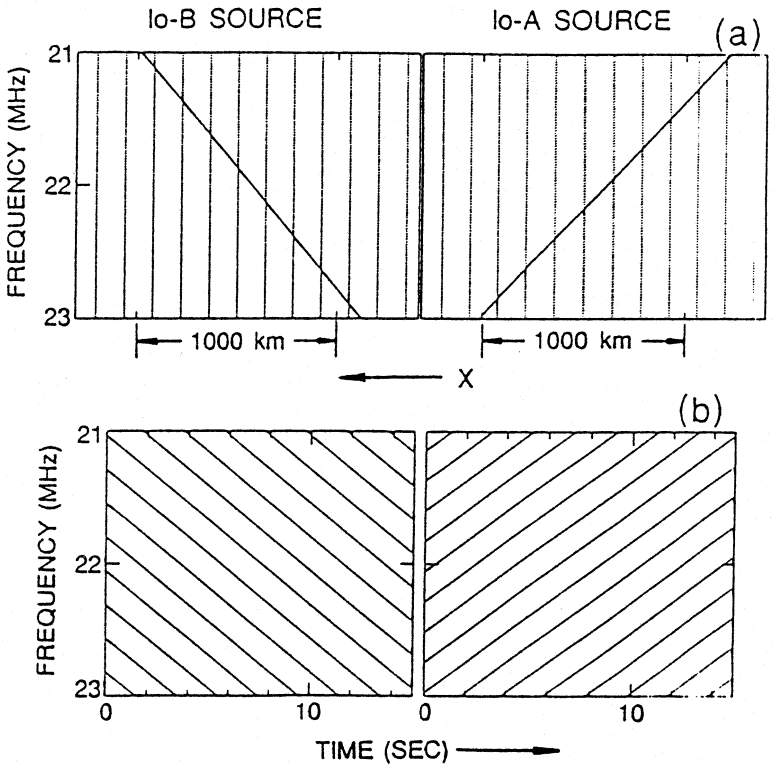

Figure 6: a) The diagonal smooth lines are plots of the emission frequencies at positions along the PEFT (for Io–B and Io–A) vs the westward distances, x, of the projections of these positions on a plane perpendicular to the line of sight. The vertical dotted lines indicate the x–positions of successive field–aligned plasma column center lines for incident rays at frequencies indicated on the vertical scale. b) Resulting frequency–time curves of the modulation lanes produced by the rays penetrating the plasma column interference screen.

centers are $2\theta_1$ apart, and the relationship between θ_1 and the electron density in the columns is given by Equation (4.1).

In the above model for producing the lobe pattern, it is clear that intensity maxima and minima occur at a given frequency with increasing time as the source–Earth line alternately crosses columns and the spaces between them. The modulation lane pattern observed at a single frequency is simply the multilobed intensity vs time curve at Earth due to our model for that frequency. At constant time, on the other hand, an intensity maximum occurs at each frequency corresponding to an altitude in the northern end of the PEFT for which the source–Earth line penetrates the center of a column. The projection of this part of the PEFT as viewed from Earth is tilted with respect to the plasma columns, as is suggested in Figure 10*a* for Io–B and Figure 6 for both sources. It can be seen from Figure 6 that the source–Earth lines from many altitudes in the PEFT may penetrate different columns at the same time. Thus there may be many alternating intensity maxima and minima at different frequencies at a given time. It is this effect that gives rise to the slopes of the dynamic spectral modulation lanes.

We now make calculations on the basis of the model that has been presented. We assume a coordinate system in which the line from the center of Jupiter to the observer on Earth is fixed. Due to magnetospheric rotation, the velocity, v_c, of the plasma column system (which is mainly in a direction perpendicular to both the column lengths and the Jupiter–Earth line) is approximately 74 km/sec. As the source follows Io's orbital motion, the component of its velocity perpendicular to the Jupiter–Earth line, v_s, is typically about 7 km/sec for both Io–B and Io–A. The angular velocity of the plasma column system about the source is given by $\Omega = (v_c - v_s)/r = 1.9 \times 10^{-4}$ rad/sec, in which r, the distance from the source to the columns, is about 5 R_J. Each modulation maximum

occurs when a column center crosses the source–Earth line. The observed time intervals, Δt, between successive modulation maxima at fixed frequencies are typically 2 sec. The angular separation between adjacent columns as seen from the source, α, equals $\Omega\Delta t$. The distance between columns is thus

$$d = r\alpha = r\Omega\Delta t \approx 68\Delta t \ \ (\mathrm{km})\,. \tag{4.2}$$

A fixed–frequency modulation period of 2 sec indicates a column separation of about 140 km. It can be seen from Figure 5 that α is twice θ_1, where θ_1 is the angle from the undeviated ray direction to that for which the E field has been reduced by one–half. Thus $\theta_1 = 0.95 \times 10^{-4}\,\Delta t$. For $\Delta t = 2$ sec, θ_1 is 1.9×10^{-4} rad, or $40''$ of arc.

For the highest degree of cancellation of a direct ray passing nearly midway between columns (e.g., B in Figure 5) by the rays scattered from two adjacent columns (b_4 and c_2), the latter two rays must each differ in phase by 180° from the direct ray (B). In this case we have the relationship $r - \sqrt{r^2 - (d/2)^2} = \lambda/2$. Here, d is the distance between column centers, r is the distance from the point source to a column, and λ is the wavelength. To a very close approximation, the above equation becomes

$$d^2 = 4\lambda r\,. \tag{4.3}$$

The wavelength at which this equation is most nearly exact (for a given d value) is also very nearly that for which the scattered ray from each adjacent column (like a_5 and c_1 in Figure 5) adds with 360° phase difference with the ray through the center of the intermediate column (b_3). Thus the intensity maxima are highest and the minima are lowest at the wavelength λ, producing the greatest modulation depth.

By eliminating d from Equations (4.2) and (4.3), and letting $r = 5\,R_J$, we obtain the expression for the optimum frequency, or frequency of greatest modulation depth. It is $f_1 = 80 \times 10^6/(\Delta t)^2$ (Hz). This is the frequency at which we would expect modulation lanes to be most easily discernible. Assuming Δt to be 2 sec, we obtain a frequency of about 20 MHz. This is in quite good agreement with the fact that most modulation lanes have been observed in the vicinity of 20 to 23 MHz. When the intercolumn distance changes, the optimum frequency and the lane time spacing would be expected to change accordingly. When the observing frequency is a few MHz above or below the optimum frequency, our model predicts that the lane time spacing should not change. However, the intensity maxima would be lower and the minima higher, reducing the depth of modulation by amounts that increase as the departure of the frequency from the optimum, f_1, is increased.

We now calculate the value of the mean electron density fluctuation within the columns, ΔN_1, required to produce the scattering angle $\theta_1 = 1.9 \times 10^{-4}$ rad (i.e., $40''$). From Equation (4.1) we have $\sqrt{w/s}\,\Delta N = \theta f^2/40.5$. Inserting $f_1 = 20 \times 10^6$ Hz and the above value of θ_1, we have the relation (corresponding to the case for which $\Delta t = 2$ sec), $\sqrt{w/s}\,\Delta N \approx 1.9 \times 10^9$. Let us arbitrarily assume that the column diameter, w, is 0.2 d, or 30 km. Even more arbitrarily, let us assume that the mean separation between plasma irregularities within the columns (for which the mean electron density fluctuation is ΔN_1) is 0.3 km. We then have $\Delta N_1 = 1.9 \times 10^8$ electrons/m^3 or 190 electrons/cm^3. This seems

entirely realistic. It indicates that the electron density fluctuations and the smoothed ambient electron density are of about the same order of magnitude.

Although the most probable time spacing (Δt) between modulation lanes for fixed frequencies in the vicinity of 20 MHz is close to 2 sec, values ranging from 1 to 5 sec are often observed. In our model, column separations less than the previously calculated value of 140 km would result in $\Delta t < 2$ sec. However, in such cases the modulation depth would be reduced because a ray passing midway between two columns would then be less than 180° out of phase with the ray scattered in its direction from each of the adjacent columns. On the other hand, in order to obtain $\Delta t > 2$ sec we must invoke higher–order interference between the scattered and unscattered rays. Equation (4.3) is for first–order destructive interference between the direct ray in the direction midway between column centers and either of the adjacent scattered rays that are parallel to it. In deriving (4.3), if we had let the difference between the direct and scattered ray paths be $n\lambda/2$ in order to produce nth–order destructive interference in this direction, the required column separation would have been $d^2 = 4n\lambda r$. It is thus clear that higher–order interference leads to values of $d, \Delta t, \theta_1$, and ΔN_1 that have been increased by the factor $\sqrt{n}$. For example, 5th–order interference requires a value of ΔN_1 of about 420 electrons/cm^3 in order to produce a scattering angle θ_1 of about 90″ of arc with a column separation of 310 km, thus yielding modulation lanes with a fixed–frequency time separation of 4.5 sec. We therefore interpret the more widely spaced modulation lanes as indicating denser and more widely separated field aligned plasma columns.

Next, we calculate the modulation lane frequency drift rates as predicted by our model. Consider two points on the active flux tube (PEFT) from which radiation is being emitted at the frequencies f_h and f_l, where f_h is the higher. Define the positive x direction to be perpendicular to the line of sight to Earth and parallel to the Jovian equator, in the direction of increasing System III (west) longitude. Let the x coordinates of the above two points be x_h and x_l, respectively. As stated above, the angular velocity of the plasma column system about the radio source is $(v_c - v_s)/r$, where v_s and v_c are the x–components of the velocities of the radio source and the plasma columns located between it and Earth, respectively. The mean frequency drift rate of a modulation lane over the frequency interval between f_l and f_h is defined to be $DR = (f_h - f_l)/(t_h - t_l)$. Since $t_h > t_l$ for Io–B modulation lanes and $t_h < t_l$ for Io–A, DR is positive for the former and negative for the latter. The drift rate equation can be written in the form

$$DR = -\frac{(f_h - f_l)}{(v_c - v_s)\,(x_h - x_l)}\,. \tag{4.4}$$

This equation will be used in the generation of modeled modulation lanes for comparison with observed data.

A requirement for the production of a clear pattern of modulation lanes is that the radio source size must be small in comparison with the spacing of the plasma columns in the screen. This implies that the source is considerably smaller than 140 km in the case of the most probable fixed–frequency modulation lane time separation, about 2 sec. Dulk [1970] and Lynch et al. [1972], using east–west and north–south VLBI baselines, respectively, showed that the Jovian Io–related sources are much less than 400 km in width at a given frequency. This is consistent with our upper limit requirement for modulation lanes.

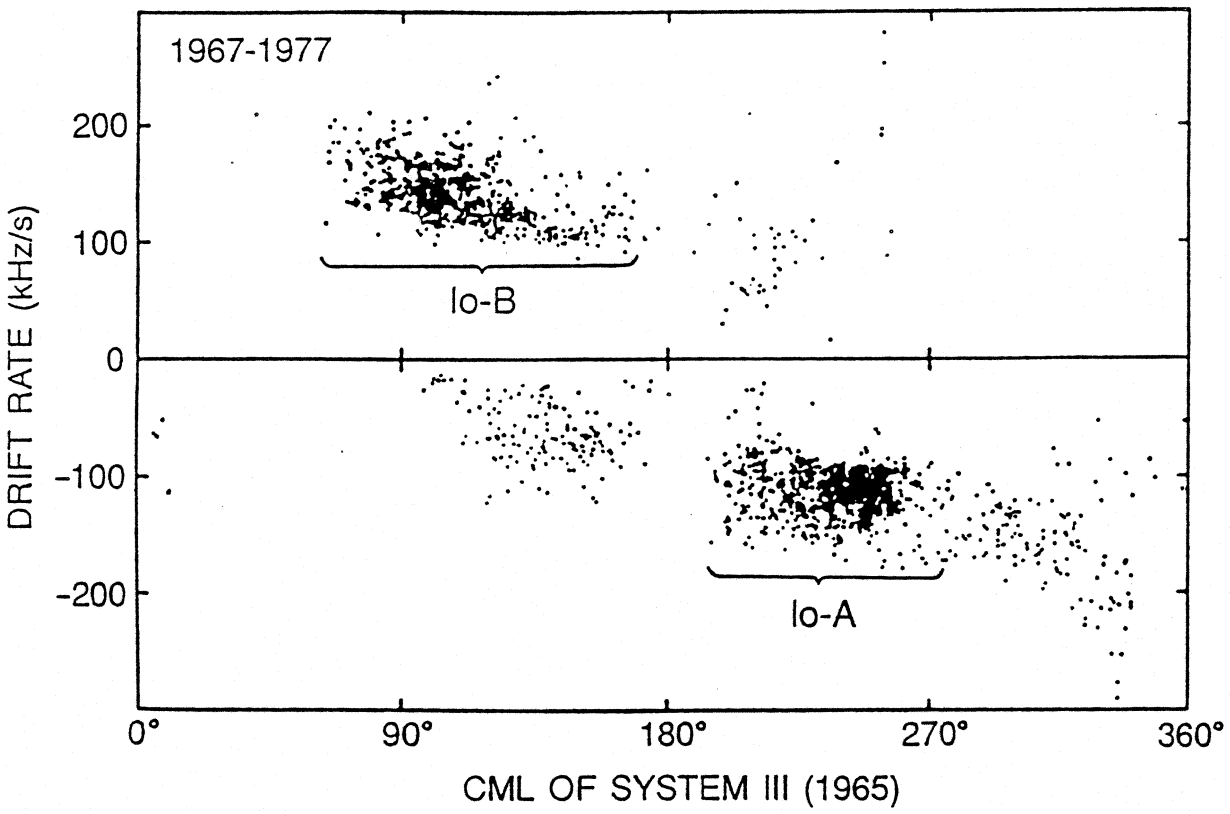

Figure 7: Frequency–time drift rates of modulation lanes of Io–related regions plotted as a function of CML during the period from 1967 to 1977, reproduced from Riihimaa [1978]. The brackets indicate the Io–B points of positive slope and the Io–A points of negative slope that constitute the so–called major component.

5 Modeling results

We have developed a quantitative model for the production of modulation lanes in which the free parameters were adjusted to provide the best fit to the dynamic spectral observations of Riihimaa [1978] and Genova et al. [1981]. Riihimaa's data consist of a plot of Io–B and Io–A modulation lane drift rates vs central meridian longitude for 10 years of observations over the frequency range from 21 to 23 MHz; it is shown in Figure 7. The data of Genova et al. that we use are dynamic spectral plots of sets of modulation lanes covering an exceptionally wide frequency bandwidth (12 MHz) and a correspondingly long time span (80 sec). One of these lanes is reproduced as the heavy line in Figure 10*b*. As is customary in recent Jovian decametric emission modeling, we assumed that the Io–related radiation at a given time is emitted from the flux tube (the PEFT) at which the Alfvén wave previously excited by its passage across Io is just arriving at the emission altitudes, the frequency emitted from each altitude being approximately the electron cyclotron frequency at that altitude. The O4 magnetic field model [Acuña and Ness, 1976] is used. To a first approximation the radiation at each frequency can be considered to be beamed into a wide–angle hollow cone, the axis of which is tangent to the magnetic field at the emission point (the latter being the cone apex). Io–B and Io–A radiation are observed when the leading and trailing limbs of the hollow–cone beam pass across

Earth. The primary adjustable parameter of our modulation lane model is the emission cone opening half–angle, which is assumed to be constant with respect to time. We define this cone angle, β, to be the angle from the cone axis (tangent to the magnetic field) to the direction of maximum emission intensity; β is constant with respect to azimuth about the cone axis. The thickness of the beam is unspecified, but is assumed to be small compared with β. The source points for the restricted range of emitted frequencies being considered here lie in the PEFT at different altitudes above its foot; they are all at nearly the same longitude, λ_P. The longitude of the observer is the same as the CML. The angle between the observer's central meridian and the PEFT is thus ($\lambda_P - $CML). For a given cone angle, there is one value of ($\lambda_P - $CML) in the Io–B CML range and one in the Io–A CML range for which radiation in our restricted frequency band is emitted in a direction that will take it to Earth. There is thus a functional relationship between cone angle, λ_P, and CML. (It should be noted that up to this point it has not been necessary to specify either Io's orbital phase or the PEFT lead angle ahead of Io.)

We now consider again the effect of the intervening interference screen. When the radiation passes through it, the previously described interference pattern is formed and modulation lanes may be observed at Earth as a result. In the continuous frequency distribution of the emission from the PEFT, the frequency increases with decreasing altitude above the flux tube foot. The projection of this active part of the PEFT on the plane of the interference screen (which is nearly normal to the line of sight) is tilted with respect to the field aligned plasma columns. The tilt directions are opposite for Io–B and Io–A. If we define the x–axis to be increasing in the direction of increasing longitude (so that it is normal to the line of sight and nearly so to the plasma columns), different frequency components within the bandwidth of a radio receiver on Earth will have originated from different x values of the PEFT at a given time. Thus there may have been intensity lobe maxima at some of the received frequencies and lobe minima at other frequencies at this time. Since the x–component of velocity of the screen is much greater than that of the radiating PEFT, the frequencies of the intensity maxima and minima will increase or decrease as time increases, depending on the direction of tilt of the projected PEFT with respect to the plasma columns. The dynamic spectrum of this band of frequencies is thus a set of modulation lanes. The frequency drift rates of the lanes are given in terms of geometrically calculable quantities by Equation (4.4).

For each of a series of values of λ_P, we computed cone angle (β) and frequency drift rate (DR) vs CML, for frequencies between 21 and 23 MHz. The drift rate is shown as a function of CML for each of several cone angles in Figure 8. We have shaded the region between the β values 55° to 65° for the Io–B curves and between 55° and 70° for the Io–A curves. These shaded regions for the model results match the densest regions of observed drift rate points in Figure 7 surprisingly closely for Io–B, and very well but not quite so closely for Io–A. It thus appears that the most probable value of β for both Io–B and Io–A is about 59°. If the $\beta = 59°$ curve were plotted on Figure 7, it would lie within ±4° of the centroid curves of the positive–drift Io–B points in the CML range 70° to 140° and the negative–drift Io–A points in the CML range 200° to 260°.

We now consider the variation of the PEFT lead angle (LA) along the constant–β curves of DR vs CML for Io–B in Figure 8. The values of LA were determined from the corre-

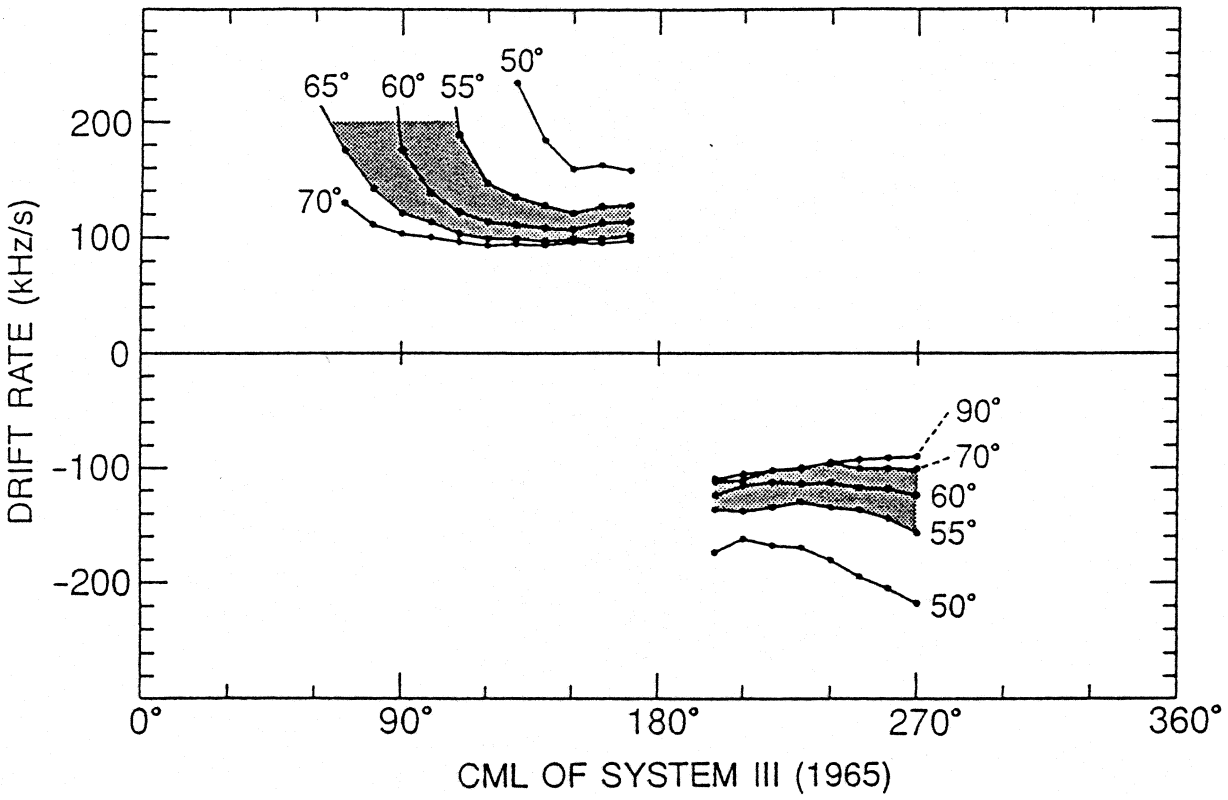

Figure 8: Calculated drift rate distribution of modulation lanes as a function of CML based on the fixed cone half–angle model. The two shaded regions between calculated curves are good fits to the densest areas of the plot of observed drift rate points in Fig. 7.

sponding λ_P values, using the formula

$$LA = 180^\circ - \Phi_{IO} - (\lambda_P - \mathrm{CML}). \tag{5.1}$$

In this formula, Φ_{IO} is Io's orbital phase from superior geocentric conjunction. During the 10 years of observations represented by the points plotted in Figure 7, the relationship between the CML vs time and Φ_{IO} vs time curves varied somewhat for Io–B radiation and more so for the Io–A radiation. We can assume, however, that Φ_{IO} for most of the Io–B points was 90° (with an average error of perhaps 5° or 10°), enabling us to calculate LA vs CML for the Io–B longitude range. The result is displayed in Figure 9. It is apparent that LA varies with CML if β is constant. A variation would be expected, since LA depends on the mean Alfvén wave propagation velocity between Io and the radio emission altitude within the PEFT, which in turn varies with the mean electron density. The mean electron density would be expected to vary considerably as λ_P changes with time. For the most probable cone angle, about 60°, it is seen that the PEFT lead angle varies from about 40° to 70° across the Io–B CML range.

As stated earlier, Genova et al. [1981] were able to obtain individual modulation lanes spanning frequency ranges as great as 12 MHz, the corresponding lifetime of an individual lane being about 80 sec. This was made possible by the wide–bandwidth high–gain Meudon decametric antenna array, operated in daylight near the time of sunspot minimum when Jupiter was only 12° from the Sun. At such a small solar elongation angle

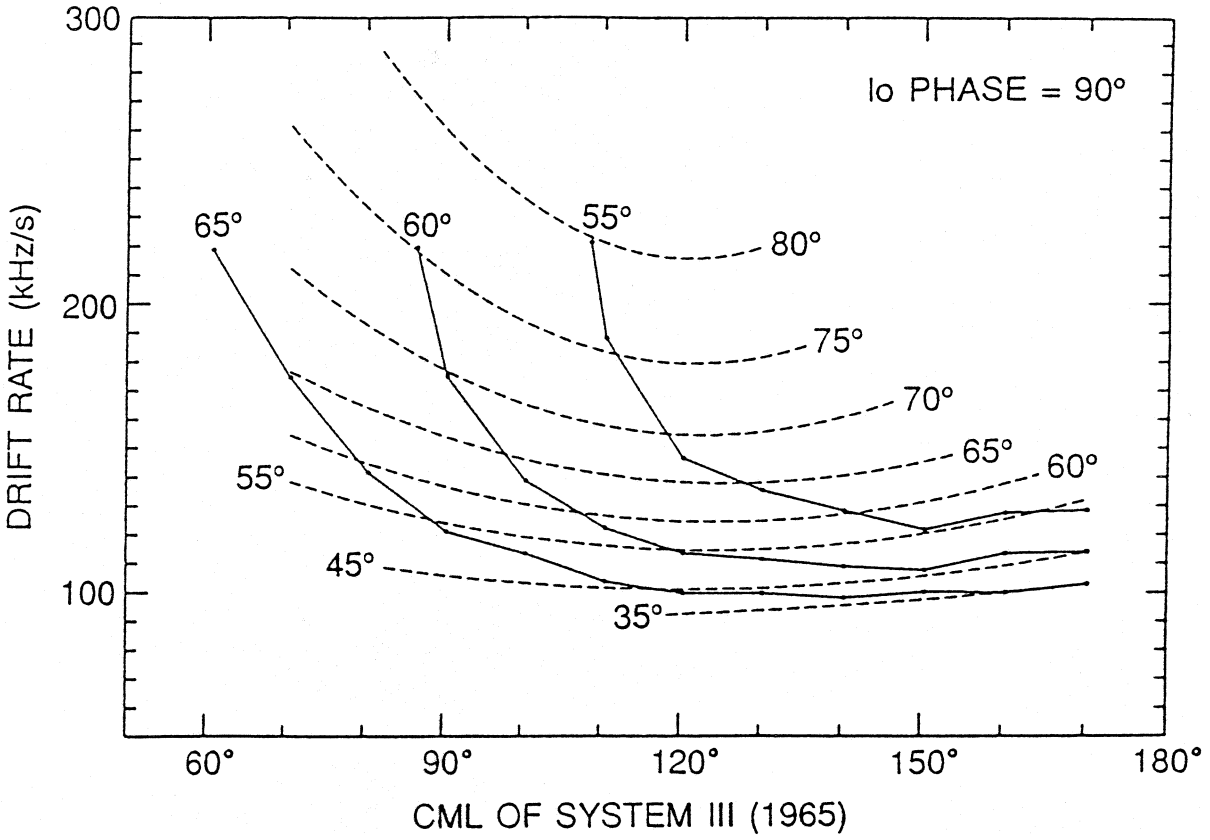

Figure 9: Calculated drift rate curves for Io–B. The solid lines are contours of constant cone half–angle, and the dotted lines are contours of constant lead angle of the PEFT ahead of Io. It was necessary to assume a value of Io's orbital phase in order to calculate the lead angle; the assumed value was 90°.

and low level of solar activity, the extremely deep interplanetary scintillation of Jovian radiation responsible for the L burst waveform nearly vanishes, ionospheric scintillation is greatly reduced, and low–frequency terrestrial interference is at a minimum. Such conditions provide the relatively long intervals of nearly constant interference–free Jovian emission intensity needed for the observation of very wide–band modulation lanes. It is most instructive to simulate these modulation lanes by means of our model. Figure 10*a* indicates in perspective the PEFT for Io–B emission, the altitudes from which emissions at frequencies of 10, 20, and 30 MHz occur, and the relative orientations of the field–aligned plasma columns that produce the modulation lane interference pattern. The heavy line in Figure 10*b* is a frequency–time plot of one of the wide–bandwidth modulation lanes observed by Genova et al. (as presented in their Figure 9), extending from 20 to 32 MHz. We proceeded as follows in modeling this event.

Due to the brief lifetime of the event, CML, Φ_{IO}, the PEFT longitude (λ_P), and the PEFT lead angle (LA) were all constant; CML was 133° and Φ_{IO} was 96°. In general at a given frequency, λ_P, cone angle (β), and CML are interrelated; any one can be determined from the other two. However, since λ_P was essentially constant over the frequency range from 20 to 32 MHz, and CML is a known constant, we can calculate β if we assume λ_P (and vice versa). And since LA is calculable from Φ_{IO}, λ_P, and CML by means of Equation (5.1), β

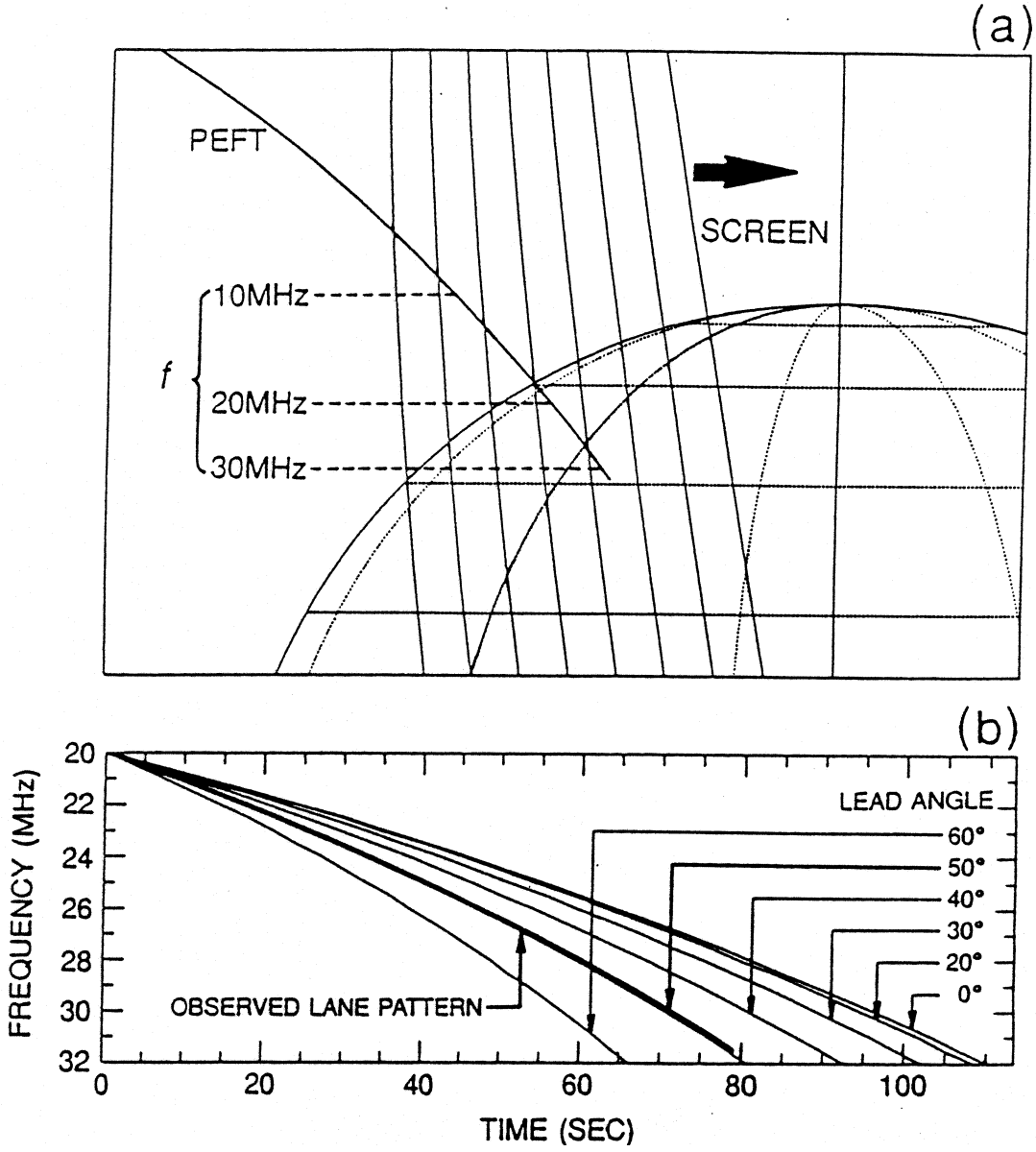

Figure 10: a) PEFT as viewed from Earth through the interference screen. Emission frequencies in the PEFT are indicated. The geometry is the same as for Fig. 2. b) The thick line is a reproduction of the frequency–time curve of a typical very wide bandwidth modulation lane observed by Genova et al. [1981]. The curves represented by thinner lines were calculated from the model for the various indicated values of assumed lead angle. It should be noted that the calculated curve for 50° lead angle is indistinguishable from the observed curve.

can be expressed as a function of LA. The frequency drift rate (DR) at a given frequency can be found from β and (λ_P−CML), with the aid of Equation (4.4). Our procedure was therefore to assume a value of LA, calculate λ_P and β, calculate mean values of DR for 0.5 MHz frequency increments from 20 to 32 MHz, and plot the frequency vs time curve for that LA value. The process was repeated for each of a series of LA values. The resulting plots for lead angle values from 0° to 60° are shown in Figure 10*b*.

It is clear that the modeled frequency vs time curve of an interference intensity maximum in Figure 10*b* corresponding to a lead angle of 50° provides a very close fit to the actual modulation lane, accurately reproducing its curvature. The existence of the curvature of modulation lane patterns was first pointed out by Riihimaa [1970]. Genova et al. [1981] verified the curvature, and reported that the curvature sense is always such that the absolute value of the frequency drift rate decreases with increasing frequency. Corresponding to the 50° lead angle, the value of λ_P was 167°, and the cone half–angles at the frequencies 22, 26, and 30 MHz were 58.3°, 59.1°, and 59.6°, respectively. We also successfully simulated the dynamic spectrum of one of the modulation lanes from another group obtained by Genova et al. [1981] (illustrated in their Figure 1*b*). In this case, CML was 142° and Φ_{IO} was 89°. The modeled lead angle was 54°, and the cone half–angles at the frequencies 22, 26, and 30 MHz were 58.0°, 58.7°, and 59.2°, in remarkably close agreement with the previous result. It appears that our modulation lane model used in conjunction with wide–band high–gain observations of the type obtained at Meudon is capable of providing a wealth of information on the modulation lane phenomenon and the environment in which it originates.

6 Summary and conclusions

We have shown that the assumed interference screen consisting of field aligned columns of enhanced plasma density located downstream from Io can account for the modulation lanes observed during both Io–B and Io–A Jovian decametric storms. In order to produce modulation lanes having the most frequently occurring fixed–frequency time separations, about 2 sec, plasma column separations of about 140 km and electron densities of a few hundred electrons/cm^3 in excess of the ambient value were required. The customary assumptions regarding the emission source were made, that *a*) at a given time the longitude of the radio–emitting flux tube (*i.e.*, the PEFT) is at some lead angle ahead of Io, *b*) the emission at different frequencies originates at different altitudes above the northern foot of the active flux tube, at approximately the local electron cyclotron frequency in each case, and *c*) the radiation at each frequency is emitted through a hollow–cone beam. Using the cone half–angle of the beam as the adjustable parameter of the model, we found that a value of 59° provided the best fit (an excellent one) to Riihimaa's plot of modulation lane drift rate vs central meridian longitude based on 10 years of observations between 21 and 23 MHz. The corresponding lead angle of the active flux tube ahead of Io was found to vary from 40° to 70° across the Io–B range of central meridian longitude. We attribute this variation to differences in the mean Alfvén wave velocities within the succession of active flux tubes from Io down to the radio emission region, which in turn is due mainly to differences in the average plasma density in these flux tubes. We therefore believe that our model is capable not only of accounting for the modulation lanes, but also of providing measurements of emission cone half–angle, lead angle, and mean Alfvén wave velocity and plasma density in the active flux tubes. This appears to us to be the best if not the only method presently available for making such measurements from Earth. The model also makes possible the reducing of the previous upper limit on the source width that was established from VLBI measurements. We estimate that the source width in the direction perpendicular to the plasma columns is less than 70 km.

The model was also used to fit the extremely wideband modulation lanes recorded by Genova et al. [1981] using the Meudon decametric radio telescope during ideal observing conditions. In this case the lead angle of the active flux tube ahead of Io was used as the adjustable parameter of the model, and it was systematically varied in order to find best fits to the frequency–time plots of two representative modulation lanes that were observed on different dates. The best–fit lead angle was found to be 50° for one observation date and 54° for the other. In both cases the fit of the modeled lane to the observed one was very close. Frequency–time plots of these exceptionally wideband long–duration lanes always display a characteristic curvature, which was accurately matched by the model. The derived emission cone half–angles on the two observation dates, respectively, were 58.3° and 58.0° at 22 MHz and 59.6° and 59.2° at 30 MHz. Thus, our measurements of cone half–angle at about 22 MHz were 59° from the 10 years of Riihimaa drift rate vs CML data, and 58.3° and 58.0° from the Genova et al. [1981] frequency vs time plots obtained on two different observation dates. This is indeed close agreement.

Despite these promising results, further verification will be of course necessary before the validity of the model for producing modulation lanes can be established. For example, our findings regarding the emission cone half–angle and results based on Voyager observations, also based on unproven models, must be reconciled. A definitive test of our basic idea of field–aligned plasma striations at Io's orbit might be accomplished by the Galileo spacecraft, provided it is able to make extensive plasma density measurements in the vicinity. Whether ultimately proven right, wrong, or partly right, we believe that our proposed model will provide the stimulus for renewed activity in the field.

Finally, we must address the matter of the modulation lanes that are observed in storms unrelated to Io's orbital phase, and also those Io–B and Io–A modulation lanes with atypical drift rates. Most of the Io–unrelated storms occur in the source A zone of central meridian longitude, and are classified as Non–Io–A storms. We foresee no problem in explaining the Non–Io–A modulation lanes that have frequency drift rates similar to those of Io–A storms. The explanation of the relatively small but distinct body of lanes possessing atypical drift rates may be more difficult, however. Included in this category are the Io–B lanes with negative drift rates, the Io–A lanes with positive drift rates, and others that have drift rates of the correct sign but of absolute values that are much too small. We will consider the hypothesis that these are produced by field–aligned interference screens at other locations than Io's orbit, where the angular velocity of the screen about Jupiter's rotation axis is less than that of the screen at 6 R_J, and in some cases less than the angular velocity of the foot of the active flux tube about Jupiter's axis. Another possibility is that they are caused by interference of radiation scattered from drifting plasma clouds or even waves located farther out in the magnetosphere, in the region in which corotation has ceased. There are very likely other possibilities which should also be considered.

Acknowledgments: We would like to express our thanks to Dr. F. Reyes and Mr. W. B. Greenman for fruitful discussions. This study was made while one of the authors (K. I.) was in residence at the University of Florida, Department of Astronomy, as a

visiting associate professor on the 1990 program of long term research abroad sponsored by the Ministry of Education of the Japanese Government. K. I. wishes to express his thanks for the hospitality of the University of Florida. This work was supported in part by National Science Foundation grant AST 8920861 and by National Aeronautical and Space Administration grant NAGW–2410.

References

Acuña, M. H., and N. F. Ness, The main magnetic field of Jupiter, *J. Geophys. Res.*, **81**, 2917–2922, 1976.

Carr, T. D., and M. D. Desch, Recent decametric and hectometric observations of Jupiter, in *Jupiter*, edited by T. Gehrels, pp. 693–737, University of Arizona Press, Tucson, 1976.

Carr, T. D., M. D. Desch, and J. K. Alexander, Phenomenology of magnetospheric radio emissions, in *Physics of the Jovian Magnetosphere*, edited by A. J. Dessler, pp. 226–284, Cambridge University Press, New York, 1983.

Douglas, J. N., and H. J. Smith, Presence and correlation of fine structure in Jovian decametric radiation, *Nature*, **161**, 741, 1961.

Douglas, J. N., and H. J. Smith, Interplanetary scintillation in Jovian decametric radiation, *Astrophys. J.*, **148**, 885–904, 1967.

Dulk, G. A., Characteristics of Jupiter's decametric radio source measured with arc–second resolution, *Astrophys. J.*, **159**, 671–684, 1970.

Genova, F., M. G. Aubier, and A. Lecacheux, Modulations in Jovian decametric spectra: Propagation effects in terrestrial ionosphere and Jovian environment, *Astron. Astrophys.*, **104**, 229–239, 1981.

Hashimoto, K., and M. L. Goldstein, A theory of the Io phase asymmetry of the Jovian decametric radiation, *J. Geophys. Res.*, **88**, 2010–2020, 1983.

Kraus, J. D., *Radio Astronomy*, Cygnus–Quasar Books, Powell, Ohio, 2nd edition, 1986.

Lynch, M. A., T. D. Carr, J. May, W. F. Block, V. M. Robinson, and N. F. Six, Long–baseline analysis of a Jovian decametric L–burst, *Astrophys. Lett.*, **10**, 153–158, 1972.

Meyer–Vernet, N., G. Daigne, and A. Lecacheux, Dynamic spectra of some terrestrial ionospheric effects at decametric wave lengths applications in other astrophysical contexts, *Astron. Astrophys.*, **96**, 296–301, 1981.

Riihimaa, J. J., Structured events in the dynamic spectra of Jupiter's decametric radio emission, *Astron. J.*, **73**, 265–270, 1968.

Riihimaa, J. J., Modulation lanes in the dynamic spectra of Jovian L–bursts, *Astron. Astrophys.*, **4**, 180–188, 1970.

Riihimaa, J. J., Radio spectra of Jupiter, *Technical Report* S–22, Dept. of Electrical Engineering, University of Oulu, Oulu, Finland, 1971.

Riihimaa, J. J., Modulation lanes in the dynamic spectra of Jupiter's decametric radio emission, *Annales Academiae Scientiarum Fennicae*, **A VI**, 1–39, 1974.

Riihimaa, J. J., Polarization patterns in the dynamic spectra of Jupiter's decametric radio bursts, *Astron. Astrophys.*, **53**, 121–129, 1976.

Riihimaa, J. J., L–bursts in Jupiter's decametric radio spectra, *Astrophys. Space Scie.*, **56**, 503–518, 1978.

Wu, C. S., and L. C. Lee, A theory of the terrestrial kilometric radiation, *Astrophys. J.*, **230**, 621–626, 1979.

Zheleznyakov, V. V., and V. E. Shaposhnikov, Origin of 'modulation lines' in the dynamic spectrum of Jovian decameter radio emission, *Sov. Astron.*, **23**(5), 588–595, 1979.